Optical bandgap of semiconductor nanostructures: Methods for experimental data analysis

R. Raciti, R. Bahariqushchi, C. Summonte, A. Aydinli, A. Terrasi, and S. Mirabella

Citation: Journal of Applied Physics **121**, 234304 (2017); doi: 10.1063/1.4986436
View online: https://doi.org/10.1063/1.4986436
View Table of Contents: http://aip.scitation.org/toc/jap/121/23
Published by the American Institute of Physics

Articles you may be interested in

Shell morphology and Raman spectra of epitaxial Ge-Si_xGe_{1-x} and Si-Si_xGe_{1-x} core-shell nanowires
Journal of Applied Physics **121**, 234302 (2017); 10.1063/1.4985616

Crystal and band structures of ZnS, MgS, and ZnS-MgS alloys
Journal of Applied Physics **121**, 235705 (2017); 10.1063/1.4986929

Defect analysis in GaN films of HEMT structure by cross-sectional cathodoluminescence
Journal of Applied Physics **121**, 235703 (2017); 10.1063/1.4986497

Exciton center-of-mass localization and dielectric environment effect in monolayer WS_2
Journal of Applied Physics **121**, 235702 (2017); 10.1063/1.4984790

The effect of an InP cap layer on the photoluminescence of an $In_xGa_{1-x}As_{1-y}P_y/In_zAl_{1-z}As$ quantum well heterostructure
Journal of Applied Physics **121**, 235301 (2017); 10.1063/1.4985614

All-optical measurements of carrier dynamics in bulk-GaN LEDs: Beyond the ABC approximation
Applied Physics Letters **110**, 253504 (2017); 10.1063/1.4986908

PHYSICS TODAY
WHITEPAPERS

MANAGER'S GUIDE

Accelerate R&D with Multiphysics Simulation

READ NOW

PRESENTED BY
COMSOL

Optical bandgap of semiconductor nanostructures: Methods for experimental data analysis

R. Raciti,[1] R. Bahariqushchi,[2] C. Summonte,[3] A. Aydinli,[2,4] A. Terrasi,[1] and S. Mirabella[1]
[1]*MATIS CNR-IMM and Dipartimento di Fisica e Astronomia, Università di Catania, via S. Sofia 64, 95123 Catania, Italy*
[2]*Department of Physics, Bilkent University, 06800 Ankara, Turkey*
[3]*IMM-CNR, via Gobetti, 101-40129 Bologna, Italy*
[4]*Department of Electrical and Electronics Engineering, Uludag University, 16059 Bursa, Turkey*

(Received 10 February 2017; accepted 3 June 2017; published online 20 June 2017)

Determination of the optical bandgap (E_g) in semiconductor nanostructures is a key issue in understanding the extent of quantum confinement effects (QCE) on electronic properties and it usually involves some analytical approximation in experimental data reduction and modeling of the light absorption processes. Here, we compare some of the analytical procedures frequently used to evaluate the optical bandgap from reflectance (R) and transmittance (T) spectra. Ge quantum wells and quantum dots embedded in SiO_2 were produced by plasma enhanced chemical vapor deposition, and light absorption was characterized by UV-Vis/NIR spectrophotometry. R&T elaboration to extract the absorption spectra was conducted by two approximated methods (single or double pass approximation, single pass analysis, and double pass analysis, respectively) followed by E_g evaluation through linear fit of Tauc or Cody plots. Direct fitting of R&T spectra through a Tauc-Lorentz oscillator model is used as comparison. Methods and data are discussed also in terms of the light absorption process in the presence of QCE. The reported data show that, despite the approximation, the DPA approach joined with Tauc plot gives reliable results, with clear advantages in terms of computational efforts and understanding of QCE. *Published by AIP Publishing.*
[http://dx.doi.org/10.1063/1.4986436]

I. INTRODUCTION

In the past decade, several studies focused on the optical properties of semiconductor nanostructures (NS). As the size of a semiconductor material is reduced below exciton Bohr radius (5 nm for Si and 24 nm for Ge[1,2]), the appearance of interesting optical features is expected due to quantum confinement effects (QCEs). Two of the most important optical properties of NS in the quantum confinement regime are the increase in the optical bandgap (E_g) and oscillator strength with the size reduction.[3] These characteristics allow tailoring of the light absorption and emission spectra, making possible the application of NS in many fields such as photovoltaics,[4] photodetection,[5–7] and optoelectronic[8,9] applications. Actually, the absorption modulation and enhancement in NS are still under investigation, since other factors[10–16] can interfere with the QCE. In fact, several studies have recently demonstrated how the optical properties of Si and Ge NS can be changed by varying several structural characteristics such as shape,[10] crystalline structure,[11,12] or the potential barriers surrounding the NS.[13–16]

For all these reasons, an accurate extraction of optical parameters from experimental data becomes crucial, in order to have a deeper and quantitative understanding of QCE. To date, a long debate has been underway on how to extract the optical bandgap from experimental data. Among different experimental techniques, UV-Vis/NIR spectrophotometry is the most widely used to measure transmittance (T) and reflectance (R) spectra. Based on R&T spectra, two steps are commonly used: (i) the absorption coefficient α is extracted; (ii) the optical bandgap E_g is determined by means of linear extrapolation with Tauc or Cody plots.[17,18] Concerning the first step, an approximate analysis exists labeled as the single pass analysis (SPA), where the incident light propagates through the film, neglecting multiple reflections at the film/substrate interface and interference. In this case, the absorption coefficient (α) following the Beer-Lambert law can be simply extracted by using the following equation:

$$\alpha = \frac{1}{d}\ln\frac{(1-R_S)}{T_s}, \tag{1}$$

where d, T_s, and R_s are thickness, transmittance, and reflectance of sample, respectively. Once the absorption coefficient spectra are extracted, the Tauc model or Cody model are commonly applied in order to extract the optical bandgap. The Tauc model is based on the constant momentum matrix approximation, so that the energy dependence of α in amorphous semiconductors is satisfactorily modelled by the following equation:

$$\alpha = \frac{B}{h\nu}(h\nu - E_g)^2, \tag{2}$$

where $h\nu$ is the energy of incoming photons, and B is the Tauc coefficient describing the efficiency in light absorption.[17] Clearly, the optical parameters E_g and B can be extracted through linear fit of $\sqrt{\alpha h\nu}$ (Tauc plot). The Cody model is based on a constant dipole matrix approximation

and a different expression for the absorption coefficient is used

$$\alpha \propto h\nu(h\nu - E_g)^2. \quad (3)$$

Now E_g is extracted through a linear fit of $\sqrt{\frac{\alpha}{h\nu}}$ (Cody plot).[18] On the choice among Tauc or Cody plots, many papers are present in the literature.[17–21] Most of them focus on the light absorption in a-Si and a-Si:H, debating on the effect and magnitude of tail states in the band gap and on the validity of Tauc[20] or Cody[21] model. Recently, the two models have been compared in sputtered Ge quantum well (QWs),[19] showing the presence of a double slope in the Tauc plot and claiming that the Cody plot is able to provide a more unambiguous determination of the optical bandgap compared to Tauc plot.[19] Actually, since the models use different approximations and the linear fit to extract E_g have been done in a large variety of energy ranges (from 0.3 to 2 eV), special care must be taken to compare the literature results. The choice itself of using the approximated expression (1) may impact on the results. In fact, neglecting reflections at the interfaces causes an increasing inaccuracy for thinner films, highly absorbing materials, and/or materials that show large difference in the refractive index with respect to the substrate.

In this work, we compare three analytical methods to extract E_g from R&T experimental data, with the final aim to show pros and cons in terms of complexity and accuracy. We used Ge QWs as they join the simplest confining structure (QW) and a semiconductor material (Ge) with a relative large Bohr radius QCE. The Ge QWs were produced by plasma enhanced chemical vapor deposition (PECVD), as they exhibit a much cleaner and sharper interface compared to Ge NS produced by sputtering techniques, allowing a stronger quantum confinement effect.[16] Moreover, the use of a high refractive index material, such as Ge, in films a few nanometers thin, is a situation that enhances the impact of the approximations, thus representing the most stringent test bed for the optical models. Both the extractions of α from R&T spectra and the determination of E_g from α are discussed. A simple method (labeled as double pass DPA) is then presented, showing that it is able to determine E_g with the same accuracy as the non-approximated method. The methods were compared also for Ge quantum dots (QDs) embedded in SiO_2, to show the validity in other confined structures. The results are linked to the effect of quantum confinement in semiconductor nanostructures, allowing the application of the methodology to a large variety of semiconductors nanostructures.

II. METHODS

For Ge QWs, a SiO_2(20 nm)/Ge/SiO_2(20 nm) structure was deposited on fused silica quartz at 250 °C by plasma enhanced chemical vapor deposition (PECVD). Different thicknesses (4, 6, 8 nm) of Ge film were obtained by varying the time of deposition and keeping constant the flux of GeH_4. One reference Ge film, 120 nm thick, was also grown without the presence of a SiO_2 buffer layer. The atomic Ge content and the thickness of the films were evaluated by Rutherford backscattering spectrometry (RBS), using a 2.0 MeV He^+ beam in glancing detection configuration (backscattering angle of 105°) to enhance the depth resolution, and employing SIMNRA software.[22] Transmittance and reflectance spectra were acquired using a Varian Cary 500 double beam scanning UV/visible/NIR spectrophotometer, as described in Refs. 11 and 23. For Ge QDs, thin films containing Si:Ge:O alloy were deposited by PECVD (∼300 nm thick) on fused silica quartz, followed by thermal annealing at 800 °C for 1 h to induce the precipitation of the excess of Ge in QDs. Raman spectroscopy performed on annealed samples at 800 °C revealed the presence of a considerable fraction of amorphous Ge QDs while Transmission Electron Microscopy (TEM) analysis estimated a QDs mean size of 8 nm.[23] TEM electron energy loss spectroscopy (EELS) analysis also excluded the presence of other aggregates as Si and SiGe QDs.[16] Here, we briefly review the three models used for the extraction of optical bandgap in our samples [Fig. 1(a)].

The accurate model, known as Jellison Tauc Lorentz model (labelled as JTL model in the following), is based on

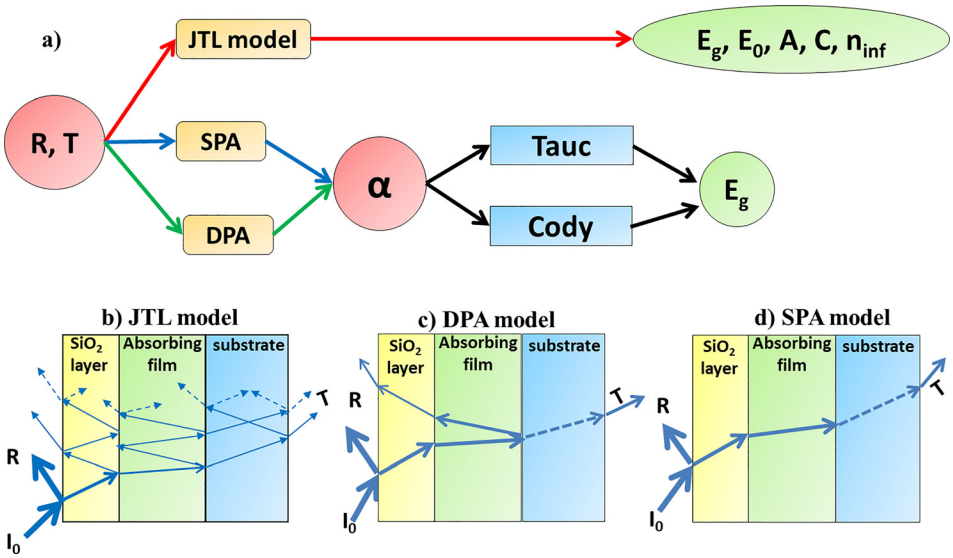

FIG. 1. (a) Schematic picture of methods for extraction of optical bandgap E_g: JTL method (red path) and approximated methods [DPA (violet path) and SPA (blue path)]. Drawing of light paths in JTL (b), DPA (c), and SPA (d) models.

the simulation of the R&T spectra by means of the Generalized Transfer Method (GTM),[24] which takes into account the reflection and transmission at all interfaces, and makes use of the complex spectral refractive index of the involved materials (film and substrate). The complex spectral refractive index of the unknown film is modeled by means of the Tauc-Lorentz approximation, in the form proposed by Jellison and Modine in 1996.[25] In this method, the imaginary part of the dielectric function (ε_2) is determined by combining a single classical Lorentz oscillator with the absorption decay deriving from the Tauc joint density of states. The Tauc-Lorentz approximation can be considered an accurate way of modelling light absorption in amorphous semiconductor thin films. On the basis of this model, the imaginary part of dielectric function ε_2 is given by the following expression:[25–27]

$$\begin{cases} \varepsilon_2 = \dfrac{1}{E}\dfrac{AE_0C(E-E_g)^2}{\left(E^2-E_0^2\right)^2+C^2E^2} & for\ E > E_g \\ \varepsilon_2 = 0 & for\ E < E_g, \end{cases} \tag{4}$$

where E_g is the band-gap of the material, A is the oscillator amplitude, E_0 is the energy position of the Lorentz peak, and C is the broadening parameter. The real part ε_1 of dielectric function is derived from the expression of ε_2 using the Kramers and Kronig integration, as follows:[25–27]

$$\varepsilon_1 = \varepsilon_1(\infty) + \frac{2}{\pi}\cdot P\cdot\int_{E_g}^{\infty}\frac{\xi\cdot\varepsilon_2(\xi)}{\xi^2-E^2}d\xi, \tag{5}$$

where the P stands for the Cauchy principal part of the integral and an additional fitting parameter $\varepsilon_1(\infty)$ has been included. The fit parameters of this model are five [E_g, E_0, A, C, and $\varepsilon_1(\infty)$] leading to the (n,k) spectra which are used, through the general transfer method, to simulate R&T, which are then compared to the experimental ones. Iterative fitting cycles based on χ^2 minimization are then used to determine the set of parameters that supply the best fit between simulated and experimental R&T spectra. The fitting was performed using the GTB-fit computer programme,[26] which is based on the Optical code.[24] Both programmes are open source and available online. Further details can be found in Refs. 24–26. A sketch of the procedure is illustrated in Fig. 1(b).

The SPA and DPA, shown in Fig. 1, are approximated methods, as the absorption coefficient spectrum is directly extracted from experimental R&T data, by partially or totally neglecting the multiple reflections and interference effects. In the SPA model [blue arrows in Fig. 1(a)] even the first reflection at film/substrate interface is neglected, as reported in Fig. 1(d). So, the absorption coefficient can be extracted by using Eq. (1). In DPA model [green arrows in Fig. 1(a)], the first reflection between absorbing thin film and substrate, if any, is taken in account, as reported in Fig. 1(c). In this way, the absorption coefficient spectra can be expressed as follows:

$$\alpha = \frac{1}{d}\ln\frac{T_{sub}(1-R_S)}{T_s}, \tag{6}$$

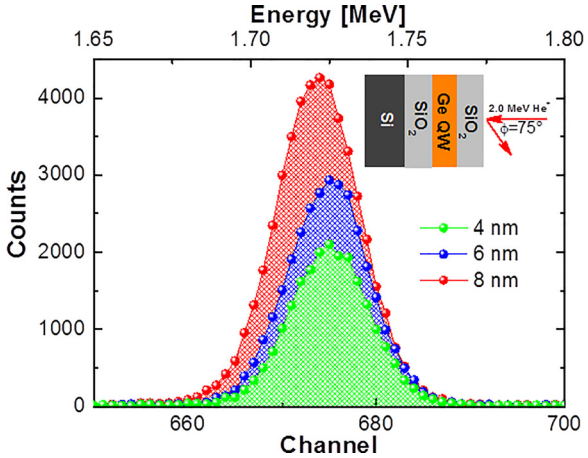

FIG. 2. RBS spectra of a-Ge QWs. The inset image represents the schematic of experimental setup.

where T_{sub} is the substrate transmittance.[11] Once the absorption coefficient spectra is calculated through Eq. (1) or (6), Tauc or Cody plots are applied to extract optical bandgaps through linear fit. In summary, in the above three methods, E_g is extracted in different ways. In JTL method, the Tauc gap E_g is a fitting parameter of the R&T spectra. In the other methods, E_g is obtained by linear fitting (Tauc or Cody plots) of α extracted directly from R&T data (DPA or SPA methods) or calculated by (n-k) dispersion derived by fitting R&T (GTM methods). In the following, JTL, DPA, and SPA methods will be compared on experimental data of Ge QWs and QDs.

III. EXPERIMENTAL DATA

Figure 2 reports the RBS data in the 1.68–1.78 MeV energy range, which are relative to He^+ backscattered by Ge atoms. The peak area is proportional to the Ge atomic dose contained in each QW. The extracted Ge dose of our samples varied from 1.7×10^{16} at/cm^2 for the thinnest film to 3.6×10^{16} at/cm^2 for the thickest one. By assuming the density for monocrystalline Ge (4.4×10^{22} at/cm^3) for the deposited material, the thickness of each sample was estimated as

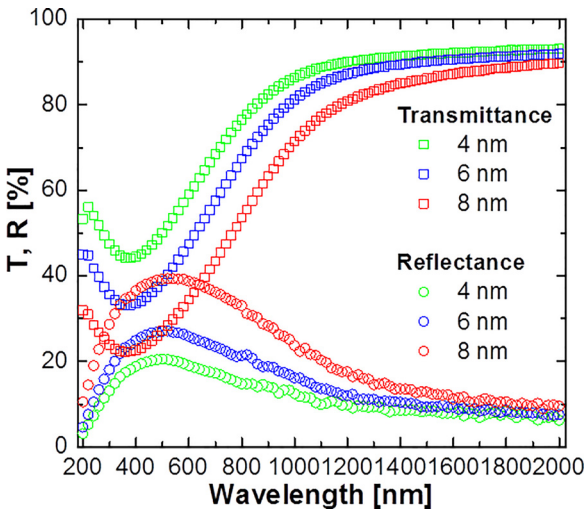

FIG. 3. Experimental T and R spectra of 4, 6, and 8 nm Ge QW.

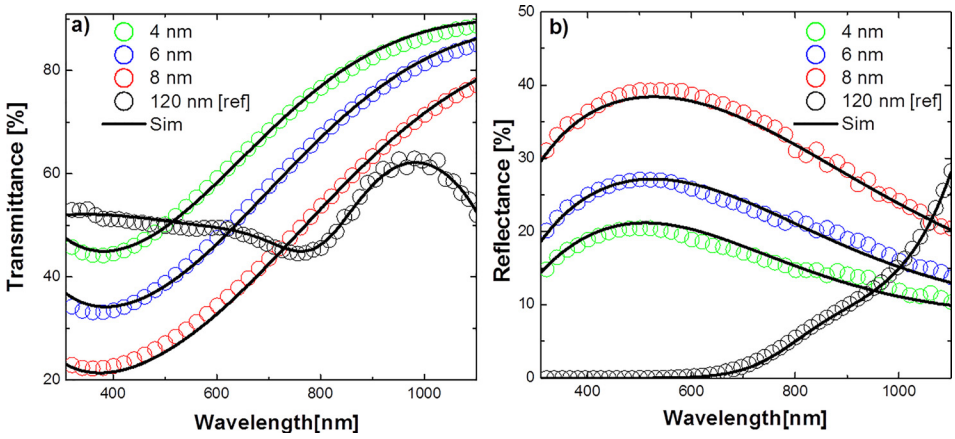

FIG. 4. Experimental (symbols) and computed (black lines) T (a) and R (b) spectra of a-Ge QW with different thickness and of a reference sample (120 nm Ge film).

TABLE I. The five JTL fit parameters and the X^2 test of all samples.

Sample (nm)	E_g (eV)	E_0 (eV)	A	C (eV)	n_{inf}	χ^2
4	1.14	2.8	206	4.10	1.3	0.89
6	1.05	2.8	201	3.96	1.3	0.59
8	0.98	2.9	185	3.79	1.3	0.79
120	0.88	2.6	175	3.34	1.3	0.32

the ratio between the Ge dose, measured by RBS, and the atomic density of Ge. Such an approach was verified by comparison with Transmission Electron Microscopy (TEM) measurements of film thickness in similar samples.[28] The so-obtained thicknesses of Ge QWs were 4, 6, and 8 nm. The overall error on thickness, including the error on Ge dose, is about 5%.

Figure 3 reports R&T spectra of Ge films with different thicknesses. The increase in thickness produces a decrease of T in the UV-Vis region for all the investigated samples. While in the IR region $R+T=1$, in the UV-Vis region $T+R<1$ indicating that part of the incident light is absorbed by the Ge QW. In the following, experimental R&T spectra will be analyzed through the three models [Fig. 1(b)], and a comparison will then be discussed.

IV. OPTICAL BANDGAP DETERMINATION

A. JTL approach

To launch the inversion software GTB-fit,[26] the structure "SiO_2 (20 nm)/unknown film/SiO_2 substrate" was used. The interfacial SiO_2 layer is neglected, as it is optically indistinguishable from the substrate. For the unknown films, the thickness was fixed at the value determined as described in Sec. III. The optical constants of the SiO_2 layer and substrate were taken from Ref. 29. In order to set the initial guess values for five JTL parameters, we start our analysis with a reference bulk Ge sample where QCE is truly absent, but the sample structure is maintained. In this case, the Ge film was 120 nm thick. A good match between the experimental and computed R&T spectra is achieved, as reported in Fig. 4 (black symbols). The parameters providing the best fit are reported in the Table I. The optical bandgap (0.88 eV) is in very good agreement with literature data (0.8 eV),[17–28] as well as the oscillator energy (2.6 eV) which resembles the lower direct transition energy (E_1) of c-Ge (2.5 eV).[30]

For what concerns the Ge QWs simulations, the five JTL parameters have been set to initial values found in the reference Ge sample. Then, through iterative cycles, the best fit was obtained. For all samples, the set of best parameters is reported as table in Fig. 4. It should be noted that relative variation of 2%–3% in the values of A, E_g, E_0, and C does not significantly worsen the relative fit ensuring a well lower than 1.

As reported in Table I, both E_0 and E_g increase with the reduction of the Ge QW thickness. These effects are due to QCE, in agreement with literature.[31] Another significant effect due to confinement can be observed in our simulation parameters in terms of increase in the broadening parameter (C) and oscillator amplitude (A) of the Lorentz oscillator with the reduction of the QW thickness. This reflects the fact that as the QW thickness is reduced, the area under

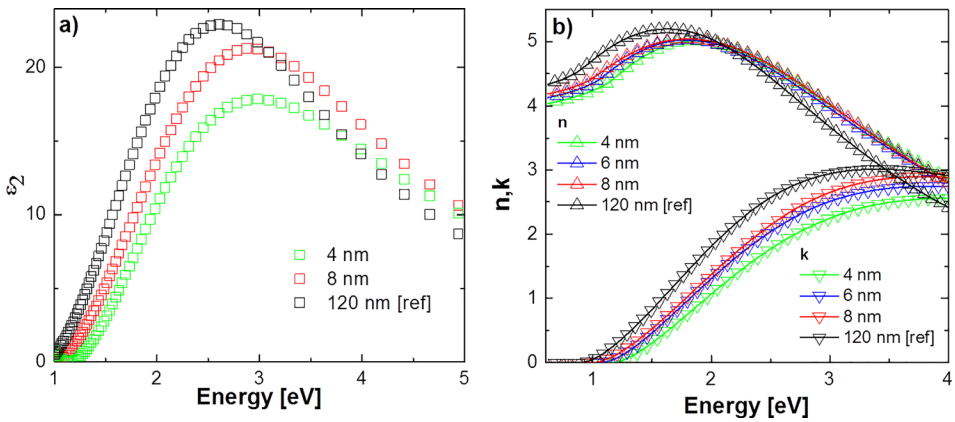

FIG. 5. ε_2 (a) and n-k spectra (b) of a-Ge films obtained by JTL model.

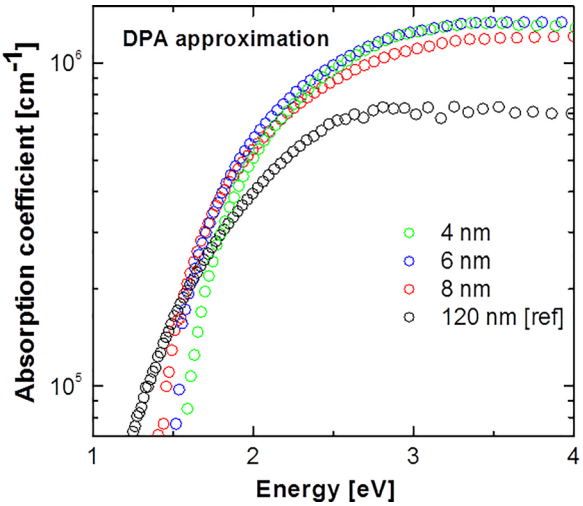

FIG. 6. The absorption coefficient of a-Ge QWs and of a reference sample extracted by DPA approach.

the Lorentz oscillator peak in the ε_2 function changes [Fig. 5(a)], as result of the modified interaction among the incoming electromagnetic field and the confined electrons, in agreement with previous observation for Ge QW.[28] The broadening of the oscillator peak can also be linked to a larger roughness of the QW. Figure 5(b) reports the n-k spectra obtained within the JTL model. The QCE induced a clear blue-shift of k spectra, linked to the bandgap widening, and a slight modification of *n* which indicates how the propagation of the electromagnetic field changes in confined Ge QW.

B. DPA approach

In this section, we show the results achieved by applying the DPA model. Figure 6 reports α spectra of a-Ge QWs and of a reference sample (120 nm thickness) as extracted by Fig. 3 after applying Eq. (6), where T^{sub} was measured by spectrophotometry in the wavelength range from 200 nm to 2000 nm. The saturation of α for the reference sample at $E > 3.4$ eV is an artifact due to the sensitivity limit of transmitted light passing through a thick absorbing layer. The most evident effect in Fig. 6 is the blue-shift occurring close to onset of absorption spectra by decreasing the QW thickness. Moreover, in the range from 1.8 eV to 2.5 eV, the magnitude of absorption coefficient in Ge QW exceeds that of 120 nm Ge film This result is in contrast with the decrease in ε_2 reported in Fig. 5 and it should be interpreted as an increasing error for thinner films deriving from the approximation.[32] Still, this artefact does not significantly alter the determination of E_g, as shown below.

TABLE II. The extracted bandgaps and energy ranges for the linear fit in Tauc and Cody plot applied to DPA method.

	Tauc		Cody	
Sample (nm)	Eg (eV)	Range fit (eV)	Eg (eV)	Range fit (eV)
4	1.16	1.7–2.5	1.27	1.6–1.8
6	1.05	1.6–2.5	0.99	1.6–1.8
8	0.96	1.6–2.4	0.85	1.6–1.8
120	0.88	1.6–2.6	0.76	1–1.3

As already reported, once the absorption spectra are calculated, the optical bandgaps can be extracted by using the linear fit performed on Tauc or Cody plots (Fig. 7).

The Tauc plot shows a much wider energy range of linearity than Cody plot, probably explaining to its wider use by the scientific community. However, choosing the right range of validity is a key issue. The linear fit in the Tauc plot were performed in an energy range determined by the empirical rule for which the Tauc model can be applied for $\alpha > 10^4\,cm^{-1}$.[17] Given the very thin film used, the rule of $3 < \alpha l < 10$ cannot be applied for the Cody plot.[21] We performed the linear fitting for both Tauc and Cody plots, in the same energy range, for all samples. In Figs. 7(a) and 7(b), Tauc and Cody plots and their relative linear fits for all the Ge QWs (from 8 to 4 nm) and reference sample are shown. Table II reports the extracted optical bandgaps and energy ranges of linear fit for Tauc and Cody plots, respectively. For Tauc plot (0.88 eV–1.16 eV) and Cody plot (0.76 eV –1.27 eV), we observe an increase in optical bandgap as Ge film thickness is reduced, as expected. The Tauc plot is characterized by a unique linear region which extends over a wider spectral range with respect to the Cody plot. This allows to perform the linear fits of the Tauc plot in a much wider energy range (1.6 eV–2.5 eV) with respect to the Cody one (1.6 eV–1.8 eV).

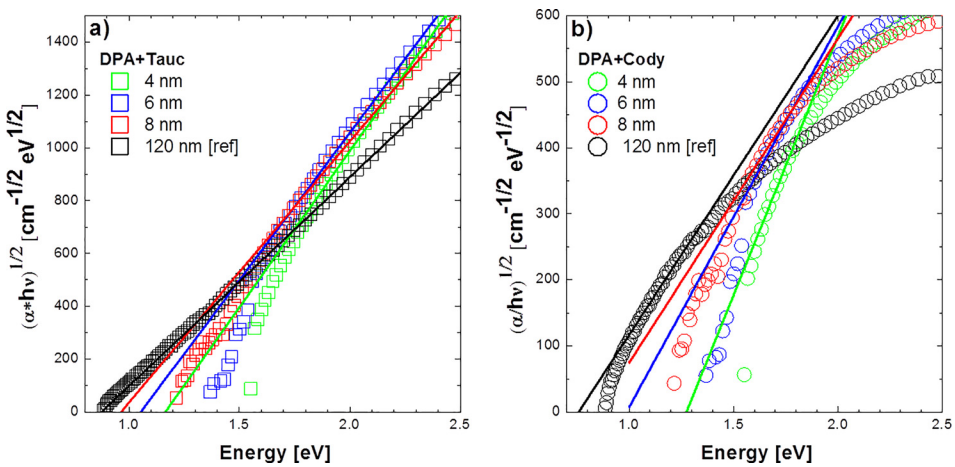

FIG. 7. Tauc (a) and Cody plots (b) and corresponding linear fit derived from data in Fig. 6.

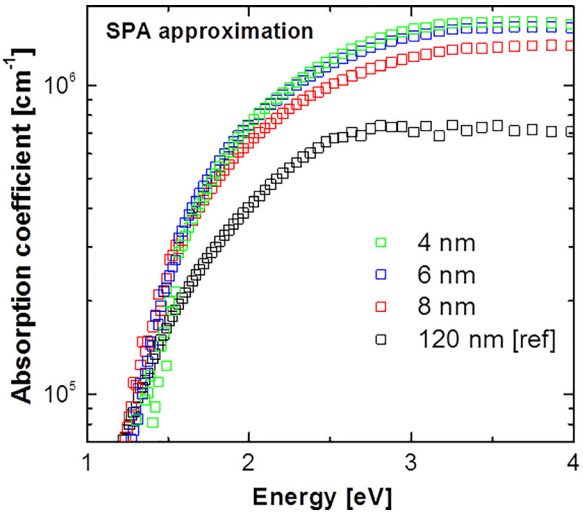

FIG. 8. The absorption coefficient of a-Ge QWs and of a reference sample extracted by SPA approach.

C. SPA approach

In Fig. 8, the absorption spectra of all Ge QWs and reference a-Ge bulk film, calculated by Eq. (1), are reported. As observed for DPA approach, the absorption onset shows a slight blue-shift with the reduction of the Ge film thickness.

In order to extract E_g, Tauc and Cody plots are used, as shown in Figs. 9(a) and 9(b). The same criteria reported in DPA section for linear fitting procedures were used here. The so-extracted values of the optical bandgap, reported in the Table III, show the expected increase with the reduction of the Ge film thickness with a larger extent for the Cody plot. As for the DPA approach, we observe that the linear region of Tauc plot is wider than for the Cody plot.

V. RESULTS AND DISCUSSION

In this section, the three methods are compared and discussed. In Fig. 10, we report the comparison of the absorption coefficient spectra for the 8 nm Ge QW, extracted with three different methods: SPA, DPA, and GTM approach. In the latter case, the α spectrum was calculated by using Eq. (6) with the k-dispersion obtained through simulation of R&T spectra. It is clear that, in both approximated methods (SPA and DPA), the absorption coefficient is overestimated in the

TABLE III. The extracted bandgaps and energy ranges for the linear fit in Tauc and Cody plot applied to SPA method.

	Tauc		Cody	
Sample (nm)	Eg (eV)	Range fit (eV)	Eg (eV)	Range fit (eV)
4	0.91	1.7–2.5	1.02	1.3–1.75
6	0.87	1.6–2.5	0.93	1.3–1.7
8	0.84	1.6–2.4	0.75	1.2–1.7
120	0.86	1.6–2.6	0.62	1–1.5

1.5 eV–4 eV energy range. This overestimation of α is due to the fact that multiple reflections and interference effects are neglected in approximated models. This discrepancy increases in the SPA approach over the DPA one and also by reducing Ge QW thickness. In fact, for thinner films, less light is absorbed in each pass and thus multiple reflections play an increasing important role on the absorption process.[32] Despite of this discrepancy, the determination of E_g by DPA converges with that of the JTL model.

In Fig. 11, the E_g extracted by JTL and approximated methods are compared. Figure 11(a) shows that JTL and DPA + Tauc methods give the same results, with a slight divergence appearing as the Ge QW goes below 4 nm. Despite the significant mismatch of absorption spectra between JTL and DPA models, the optical bandgaps extracted by both methods coincides, almost perfectly. SPA + Tauc approach gives much lower E_g values without any clear change with the thickness reduction (if E_g in the reference sample is considered). DPA + Tauc approach gives more reliable data than SPA + Tauc approach. Despite of the approximation used in DPA and SPA to extract α from R&T (as shown in Fig. 10), the first method, joined with Tauc plot, gives results comparable with the exact method. Figure 11(b) shows that the Cody plots vaguely catches the E_g increase by reducing the QW thickness, even if a large shift of 0.2–0.3 eV appears among the methods compared.

Applying the Cody plot to the approximated methods did not result in some convergence with the non-approximated method (GTM). In order to assess the reliability of approximated methods (SPA and DPA) and the application of the Cody model to these latter, we decided to compare the E_g values extracted by approximated methods coupled with

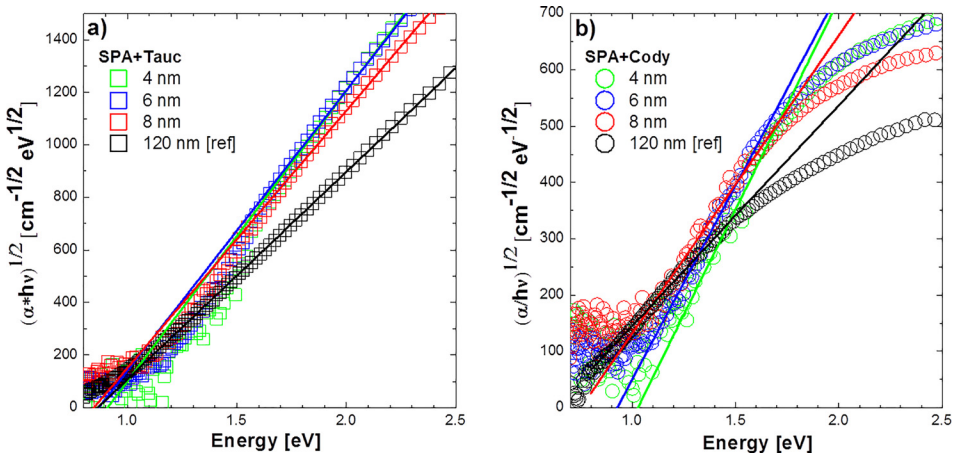

FIG. 9. Tauc (a) and Cody (b) plots and corresponding linear fit derived from data in Fig. 8.

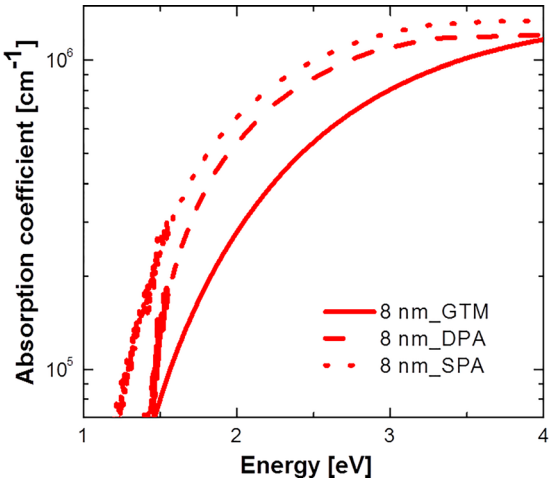

FIG. 10. The absorption coefficient spectra of 8 nm Ge QW extracted with three different methods: GTM (solid line), DPA (dashed line), and SPA (dotted line).

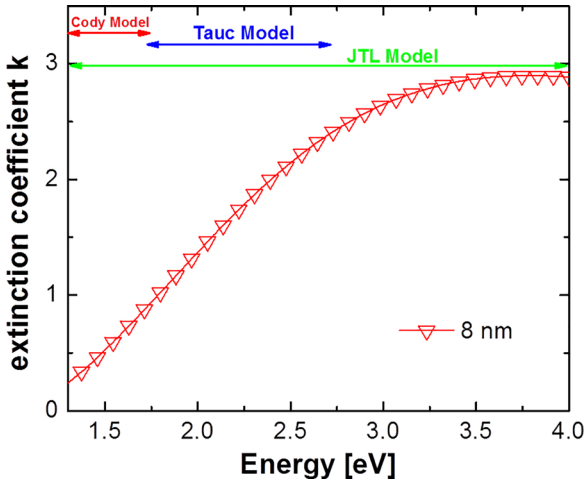

FIG. 12. Extinction coefficient k of 8 nm Ge QW with three regions of applicability of Cody (red arrow), Tauc (blue arrow), and JTL (green arrow) models.

Cody plot (DPA + Cody and SPA + Cody) with the values extracted applying the Cody plot to absorption coefficient spectra extracted through GTM approach. It should be noted that when Cody plot is used, the E_g values are usually lower than those with Tauc plot. Indeed, the reference sample analyzed with Cody plot gives invariably E_g lower than 0.8 eV (from 0.6 eV to 0.7 eV), which does not agree with theory and experimental results on a-Ge (E_g is around 0.8 eV).[17,33] It should be noted that while Cody plot gave some reliable results for a-Si,[18,21] this is not always true for other semiconductors, especially in a confined system. a-Si film is characterized by large tails in the bandgap, probably weakening the validity of Tauc assumption. Some semiconductor NSs have a high density of electronic states within the bangap, allowing a more reliable approach via the Cody plot. By studying Ge QWs grown by sputtering technique, Liu *et al.*[19] reported two linear regions of the Tauc plot, each extending over a fairly narrow energy interval (~0.3 to 0.4 eV), and a unique linear region for the Cody plots (~0.6 eV). Thus, they claimed that Cody plot gives a more unambiguous determination of E_g compared to Tauc plot.[19] Their conclusion is in contrast with ours, most probably because of the different growth technique used. In fact, Liu *et al.* prepared their Ge QWs by sputtering technique, while we used PECVD method. In a previous work, we observed that PECVD QDs exhibit a sharper interface with lower amount of Ge sub-oxide states in comparison with sputter samples, ensuring a stronger electron-hole confinement into Ge QDs of PECVD samples.[16] Since Tauc plot focuses the threshold energy range of absorption coefficient, which is affected by any midgap levels or bending induced by interface defects, the different behavior of our Tauc plots from those of Liu *et al.* can be regarded as a consequence of the different growth technique used. In our case the Tauc plot is characterized by a unique linear region which extends over a wider spectral range (0.8 eV) with respect to the case of Ref. 19. Ge NS produced by PECVD methods were shown to be almost ideal as far as the confining potential and the Ge/SiO_2 interface are concerned,[16] which can result in a lower density of tail states in the bandgap, accounting for the superiority of Tauc approach observed in our results. As already said earlier, care should be taken when considering the energy range for fitting. For this purpose, in Fig. 12, we report, as an example, the extinction coefficient spectrum *k* for the 8 nm Ge QW as obtained within the JTL model. In this graph, we identify three energy regions for the three discussed methods. The first range is for the Cody approach and goes from 1.3 eV to 1.8 eV. For energy values greater than 1.8 eV, we have generally observed the loss of linearity in the

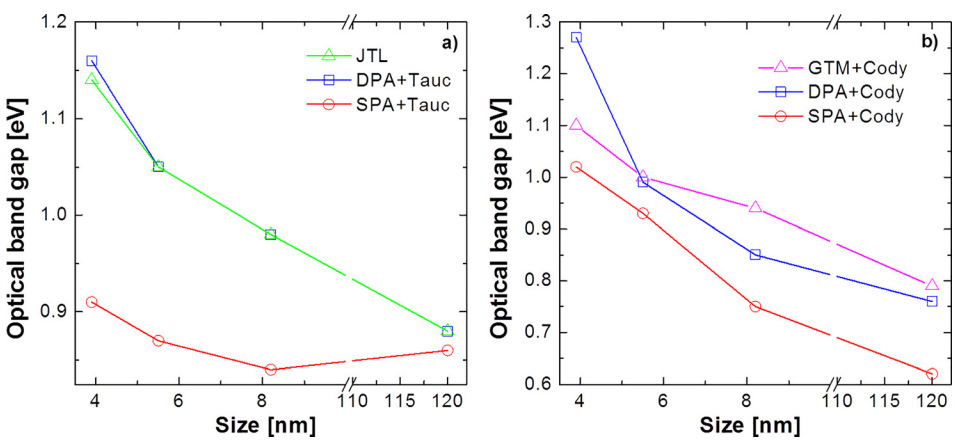

FIG. 11. (a) Comparison of optical bandgaps extracted by JTL model and by the approximated methods (DPA and SPA) by using Tauc (a) and Cody (b) plots.

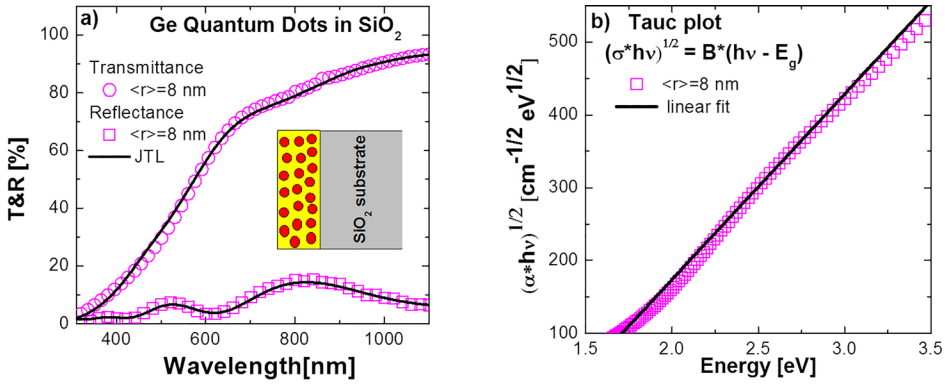

FIG. 13. (a) Experimental (symbols) and computed (black lines) T and R spectra of an ensemble Ge QDs with mean size of 8 nm. Table below reports the five JTL fit parameters and the X^2 test: (b) Tauc plot and corresponding linear fit for 8 nm Ge QDs. In the table the extracted bandgaps and energy ranges for the linear fit in Tauc plot are reported. The inset shows a schematic representation of the sample structure.

JTL parameters

Sample	E_g[eV]	E_0[eV]	A	C [eV]	n_{inf}	χ^2
<r>=8 nm	1.29	2.85	185	3.8	1.3	0.81

Sample	Tauc	
	Eg [eV]	Range fit
<r>=8 nm	1.32	2.4-2.8 eV

Cody plot. Tauc plots show a wider linear region with respect to Cody plots, ensuring a lower uncertainty in the determination of E_g through the linear fit. Finally, the application range of JTL model spreads from 1 eV to 4 eV, as the full R&T spectra have been successfully fitted. The JTL approach is clearly the most powerful one, not only because it is able to fit the experimental optical data in their full energy range but also because it does not use any approximation on the extraction of α from R&T data. Both Tauc and Cody plots show a limited energy range where the linear fit can be done, as they essentially focus on the light absorption close to the bandgap energy region. Still, Tauc approach is able to fit the approximated α over a larger range than the Cody approach, leading to smaller uncertainty in the E_g determination. Finally, Tauc model applied to α extracted through the DPA exhibited the best performance when compared to the JTL non approximated method. This is due to the larger range of linear fit of Tauc over Cody plot and the lower degree of approximation of DPA method in extraction α from experimental data.

In order to check the validity of the above results in NS other than QW, we employed a sample produced by PECVD containing Ge QD (8 nm average diameter) in SiO_2, and applied the JTL and the Tauc + DPA approach (Fig. 13). First of all, a good agreement between the experimental R&T spectra and the simulation data was obtained in this case. The fitting JTL parameters (table in Fig. 13) are consistent with the values found above for the 8 nm Ge QW (Table I), except for the E_g value which is larger for QDs, as expected given the stronger confinement (3D over 1D confined structure). The DPA + Tauc method gives the same value of E_g as the JTL one, confirming that the extraction of optical band gap via the DPA + Tauc method is reliable also for 3D confined nanostructures.

VI. CONCLUSIONS

Three methods to extract the optical bandgap of Ge NS from experimental R&T spectra have been compared to evaluate their degree of accuracy and complexity. Ge QWs (4–8 nm thick) or Ge QDs (8 nm in diameter) embedded in SiO_2 matrix were deposited by PECVD. Two methods based on double pass (DPA) or single pass (SPA) approximation are employed to extract α from R&T spectra, and Tauc or Cody plots are used to evaluate E_g by linear fitting. A third method, based on the Tauc Lorentz oscillator model, is used as a comparison where E_g comes by a direct fitting of R&T spectra by building complex refractive indexes. The DPA coupled with Tauc plot shows to be a reliable and easy method to extract E_g from R&T spectra, as its results satisfactorily converge with the exact method for Ge QWs and QDs. The SPA overestimates the absorption spectra, and as a consequence, it systematically underestimates the E_g. On the other hand, the Tauc plot always shows a much wider range of linearity in comparison to the Cody plot, leading to a better evaluation of E_g. The superiority of the Tauc approach over the Cody one, joined with the sharp and clean Ge/SiO_2 interface obtained with the PECVD technique, leads to the conclusion that the constant matrix approximation used in the Tauc model well describes the light absorption process also in confined nanostructures. The reported methods have largely been used in the literature to evaluate E_g in semiconductor NS, and our comparison between Ge QWs and QDs shows limits and benefits of each method.

ACKNOWLEDGMENTS

This work has been sponsored by bilateral CNR-TUBITAK project "Application of nanoporous Si and Ge nanostructures to advanced solar cells" (Grant No. 211T142) and in the framework of the project ENERGETIC PON00355_3391233. Part of this work was performed at BeyondNano CNR-IMM, Italy, supported by MIUR under the project Beyond-Nano (PON a3_00363). The authors thank C. Percolla, S. Tatì, and G. Panté (MATIS CNR-IMM) for expert technical assistance.

[1]F. Priolo, T. Gregorkiewicz, M. Galli, and T. F. Krauss, Nat. Nanotechnol. **9**, 19 (2014).
[2]Y. M. Niquet, G. Allan, C. Delerue, and M. Lannoo, Appl. Phys. Lett. **77**, 1182 (2000).
[3]A. D. Yoffe, Adv. Phys. **51**, 799 (2002).
[4]N. Usami, W. Pan, T. Tayagaki, S. Chu, J. Li, T. Feng, Y. Hoshi, and T. Kiguchi, Nanotechnology **23**, 185401 (2012).

[5]S. Cosentino, E. G. Barbagiovanni, I. Crupi, M. Miritello, G. Nicotra, C. Spinella, D. Pacifici, S. Mirabella, and A. Terrasi, Sol. Energy Mater. Sol. Cells **135**, 22 (2015).
[6]X. Liu, X. Ji, M. Liu, N. Liu, Z. Tao, Q. Dai, L. Wei, C. Li, X. Zhang, and B. Wang, ACS Appl. Mater. Interfaces **7**, 2452 (2015).
[7]C. Y. Chien, W. T. Lai, Y. J. Chang, C. C. Wang, M. H. Kuo, and P. W. Li, Nanoscale **6**, 5303 (2014).
[8]J. Liu, M. Beals, A. Pomerene, S. Bernardis, R. Sun, J. Cheng, L. C. Kimerling, and J. Michel, Nat. Photonics **2**, 433 (2008).
[9]Y. Kuo, Y. K. Lee, Y. Ge, S. Ren, J. E. Roth, T. I. Kamins, D. A. B. Miller, and J. S. Harris, Nature **437**, 1334 (2005).
[10]M.-F. Ng and R. Q. Zhang, J. Phys. Chem. B **110**, 21528 (2006).
[11]S. Mirabella, R. Agosta, G. Franzò, I. Crupi, M. Miritello, R. Lo Savio, M. A. Di Stefano, S. Di Marco, F. Simone, and A. Terrasi, J. Appl. Phys. **106**, 103505 (2009).
[12]R. Guerra, M. Marsili, O. Pulci, and S. Ossicini, Phys. Rev. B **84**, 075342 (2011).
[13]S. Mirabella, S. Cosentino, A. Gentile, G. Nicotra, N. Piluso, L. V. Mercaldo, F. Simone, C. Spinella, and A. Terrasi, Appl. Phys. Lett. **101**, 011911 (2012).
[14]P. B. Sorokin, P. V. Avramov, L. A. Chernozatonskii, D. G. Fedorov, and S. G. Ovchinnikov, J. Phys. Chem. A **112**, 9955 (2008).
[15]G. Franzò, M. Miritello, S. Boninelli, R. Lo Savio, M. G. Grimaldi, F. Priolo, F. Iacona, C. Spinella, and S. Coffa, J. Appl. Phys. **104**, 094306 (2008).
[16]S. Cosentino, A. M. Mio, E. G. Barbagiovanni, R. Raciti, R. Bahariqushchi, M. Miritello, G. Nicotra, A. Aydinli, C. Spinella, A. Terrasi, and S. Mirabella, Nanoscale **7**, 11401 (2015).
[17]J. Tauc, T. Grigorovivi, and A. Vancu, Phys. Status Solidi **15**, 627 (1966).
[18]G. D. Cody, B. G. Brooks, and B. Abeles, Sol. Energy Mater. **8**, 231 (1982).
[19]P. Liu, P. Longo, A. Zaslavsky, and D. Pacifici, J. Appl. Phys. **119**, 014304 (2016).
[20]S. Knief and W. von Niessen, Phys. Rev. B **59**, 12940–12946 (1999).
[21]T. M. Mok and S. K. O'Leary, J. Appl. Phys. **102**, 113525 (2007).
[22]M. Mayer, *SIMNRA User's Guide, Report IPP 9/113 Garchin* (Max Planck Institut für Plasmaphysik, 1997).
[23]S. Cosentino, E. Sungur Ozen, R. Raciti, A. M. Mio, G. Nicotra, F. Simone, R. Turan, A. Terrasi, A. Aydinli, and S. Mirabella, J. Appl. Phys **115**, 043103 (2014).
[24]E. Centurioni, Appl. Opt. **44**, 7532 (2005). The computer programme Optical can be downloaded at http://www.bo.imm.cnr.it/users/centurioni/optical.html.
[25]G. E. Jellison, Jr. and F. A. Modine, Erratum Appl. Phys. Lett. **69**, 371 (1996); **69**, 2137 (1996).
[26]A. Allegrezza, F. Gaspari, M. Canino, M. Bellettato, A. Desalvo, and C. Summonte, Thin Solid Films **556**, 105 (2014); **564**, 426 (2014).
[27]D. V. Likhachev, N. Malkova, and L. Poslavsky, Thin Solid Films **589**, 844 (2015).
[28]S. Cosentino, M. Miritello, I. Crupi, G. Nicotra, F. Simone, C. Spinella, A. Terrasi, and S. Mirabella, Nanoscale Res. Lett. **8**, 128 (2013).
[29]E. D. Palik and G. Ghosh, *Handbook of Optical Constants of Solids* (Academic Press, San Diego, 1998).
[30]M. Palummo, G. Onida, and R. Del Sole, Phys. Status Solidi A **175**, 23 (1999).
[31]S. Lee, S. Huang, G. Conibeer, and M. Green, Appl. Surf. Sci. **290**, 167 (2014).
[32]M. Schnabel, C. Summonte, S. A. Dyakov, M. Canino, L. López-Conesa, P. Löper, S. Janz, and P. R. Wilshaw, J. Appl. Phys. **117**, 045307 (2015).
[33]L. J. Pilione, K. Vedam, J. E. Yehoda, R. Messier, and P. J. McMarr, Phys. Rev. B **35**, 9368 (1987).